Phase averaged turbulence properties in the near wake of a circular cylinder at high Reynolds number using POD

Rodolphe Perrin[1,2], Marianna Braza[1], Emmanuel Cid[1], Sébastien Cazin[1], Arnaud Barthet[1], Allain Sevrain[1], Charles Mockett[2], Frank Thiele[2]

1: Institut de Mécanique des Fluides de Toulouse, allée du Pr. Camille Soula, 31400 Toulouse, France
2: ISTA, T.U-Berlin, Sekr. HF1, Mueller-Breslau Str. 8, D-10623 Berlin Germany

Abstract

The flow past a circular cylinder at high Reynolds number is studied by means of PIV, 3C-PIV and Time Resolved PIV techniques. One of the goals of this study was to allow comparisons with numerical simulations on a domain identical to that of the experiment. For this reason, the cylinder was placed in a confined environment, with a high blockage coefficient and a low aspect ratio, thereby allowing computations on a mesh of reasonable size, and avoiding 'infinite conditions'. This paper deals with the decomposition of the flow into coherent and random parts, as well as briefly presenting a comparison with Detached-Eddy Simulations (DES) of the flow. To this aim, phase averaged quantities were first obtained using the wall pressure signal on the cylinder as a trigger signal. This was achieved using both conditional sampling and LSE with similar results. This decomposition is then analysed using the Time Resolved PIV (TRPIV) measurements, as well as by comparison of the contributions of the organised and turbulent fluctuations to the time-independent Reynolds stress tensor with those obtained from velocity spectra. In agreement with other studies, it is found that the contribution of the turbulent motions is overestimated as a result of the occurrence of phase lag between the trigger and velocity signals.

A POD analysis then was performed to extract the coherent motion and to compare this decomposition with that obtained by phase averaging. Similarly to the phase averaging, the POD allows the decomposition of the time-independent stress tensor as the sum of two contributions corresponding to the first N modes, and the rest of the modes. This decomposition is then analysed by comparing these contributions to those obtained from the velocity spectra, according to the value of N chosen. It is found that these contributions are strongly dependent on N, and the contribution of the first modes greatly overestimate the coherent motion if N is too large. In order to obtain a good decomposition of the flow in coherent and random parts, the difficulty in this case lies in the choice of the number of modes.

Finally, the POD coefficients of the first two modes are used instead of the pressure signal to determine the phase of the vortex shedding, and the phase averaging is reconsidered. It is found that the phase averaged vortices are less smeared by the averaging process, the turbulent stresses better follow the evolution of the vortices, and the contributions of both coherent and turbulent fluctuations are found to agree well with those evaluated from the velocity spectra. This enhancement is obtained because the phase angle is determined directly from the velocity fields to be averaged, thereby reducing the phase-lag effect.

The comparison with DES demonstrates the high level of agreement obtainable between simulation and experiment, as well as giving an example of the kind of concrete evaluation which can be made.

1. Introduction

The flow past a circular cylinder has been the object of a considerable number of studies, as a generic bluff body flow case. These studies have shed light on the different regimes of the flow according to the Reynolds number and boundary conditions (aspect ratio, blockage, free-stream turbulence intensity, etc.). The dominant feature of this class of flow is the birth of coherent structures in the low Reynolds number range, and their persistence at high Reynolds numbers in the turbulent regime. The main structures are the von Kármán vortices, which result from a global instability, the longitudinal vortices that connect these, and which originate from a secondary

instability (e.g. Williamson (1992), Persillon & Braza (1998)), and the smaller-scaled Kelvin-Helmholtz vortices, which result from a convective instability in the shear layer (e.g. Bloor (1964), Braza (1986), Kourta (1987)). At high Reynolds number, the flow therefore presents a dual character, with organised and chaotic fluctuating motions interacting non-linearly. Accordingly, many studies have been devoted to the decomposition of the flow into its coherent and turbulent parts. As the organised motion is quasi-periodic due to the von Kármán vortices, the phase-averaging technique has been widely employed for this class of flow. Successful applications include that of Cantwell & Coles (1983) in the wake of a circular cylinder using flying hot wires, and Leder (1991) in the very near wake of a vertical flat plate using LDV. Many other techniques have been developed to extract coherent motion in a more general way. Among them, the Linear Stochastic Estimation (Adrian (1975)) allows the estimation of conditional averages from a non-conditionally acquired set of data. Furthermore, the Proper Orthogonal Decomposition (POD) technique, first introduced by Lumley (1967) in the context of coherent structures, has been increasingly applied in conjunction with domain-measurement techniques such as PIV.

Numerical simulations of such bluff body flows remain a challenge, especially near the critical regime characterised by the 'drag crisis', where the boundary layer becomes turbulent. In the context of turbulence modelling, the dual organised and chaotic character and the non-linear interactions between these must be taken into account. Therefore, a detailed data base of such a flow, allowing analysis of the dynamics of the organised and random components, direct comparisons with numerical simulations and validation and improvement of models, is of significant relevance. Providing such a data base was the main goal of this study.

To this aim, the flow considered is that past a circular cylinder at a Reynolds number of 140000, and in a confined environment with a high blockage coefficient and a low aspect ratio. This confined environment was chosen to allow direct comparisons with numerical simulations carried out on a domain of moderate size and corresponding exactly to the geometry of the experiment, by avoiding 'infinite boundary conditions'. PIV techniques were chosen because of the access to spatial information and therefore suitability to the cartography of the flow that they offer. Particular attention is devoted to the decomposition of the flow into coherent and random parts, and the analysis of the dynamics of the organised motion subjected to the turbulence. The very near wake, which is characterised by the formation of the coherent vortices, was investigated. In previous studies, the decomposition of the flow was achieved using phase averaging, using a conditional sampling procedure (Perrin & al (2005)) and also using the Linear Stochastic Estimation (Perrin & al (2006)), both giving comparable results. In both cases, the vortex shedding phase according to which the acquisitions were triggered, was obtained from the pressure signal on the cylinder. The flow was also analysed using POD in Perrin & al (2005), and comparison between the phase averaging and POD was made.

These previous studies were conducted using 2C and 3C stereoscopic PIV measurements at a low sampling rate. In this paper, the phase averaging decomposition and Proper Orthogonal Decomposition are analysed using Time Resolved PIV (TRPIV) measurements in the very near wake of the cylinder. Moreover, the phase averaging process is enhanced using the POD coefficients to determine the vortex shedding phase instead of the pressure signal used previously.

The paper is organised as follows: Section 2 presents the flow configuration, the experimental set-up of the PIV measurements, and the processing which has been performed. Section 3 briefly summarises the results of the phase averaging and POD obtained in previous studies and also deals with the analysis of both decompositions with the help of TRPIV measurements. Section 4 presents the enhancement of the phase averaging using the POD coefficients as a trigger signal. To demonstrate the value of the experiment in relationship to the goal of providing a reliable database for comparison with numerical methods, an example of such a comparison is presented in Section 5.

2. Experimental set-up and data analysis

2.1. Flow configuration

The experiment was carried out in the S1 wind tunnel at IMFT. The cylinder was mounted without endplates in a square channel of width $L=D=670$mm. The cylinder diameter is $D=140$mm, giving an aspect ratio of $L/D=4.8$, and a blockage coefficient of $D/H=0.208$ (Figure 1). As explained previously, this high confinement was chosen to allow direct comparison with numerical simulations corresponding to the exact experimental geometry. The uniform velocity Uo at the inlet was $15ms^{-1}$, which gives a Reynolds number, based on Uo and the cylinder diameter, of 140000. The free stream turbulence intensity measured by hot wire at the inlet, is 1.5%. In the following, x, y and z denote the longitudinal, transverse and spanwise directions respectively, and the origin is located at the centre of the cylinder. U, V and W are the velocity component along these directions, and all presented quantities have been non-dimensionalised using Uo and D.

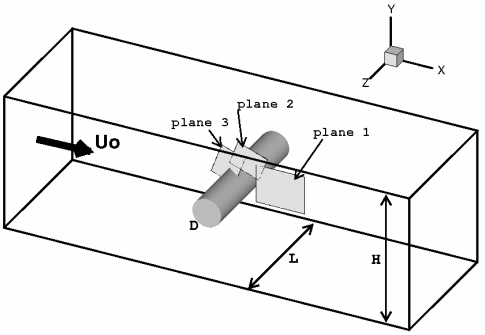

Figure 1. Configuration and measurement planes

2.2. Measurements

Details of previous low sampling rate measurements can be found in Perrin & al (2005) and Perrin & al (2006), and are briefly summarised here. Two and three component PIV acquisitions were carried out using a Nd-YAG laser Quantel (2x200mJ), PCO-Sensicam cameras of resolution 1280x1024 pixels and DEHS as seeding particles (typical size 1µm). The system, both cameras and laser, was operated at a frequency of 4Hz. The measurements were carried out in the very near wake of the cylinder and near the separation in planes located at the central span position $z/D=0$ (see Figure 1). The size of the principle measurement area (plane 1 in the near wake) was 238x188 mm ($1.7D$x$1.34D$). The particle images were analysed using an in-house development of IMFT ("Services Signaux Images"), which uses an algorithm based on a 2D FFT cross-correlation function implemented in an iterative scheme with a sub-pixel image deformation. The flow was analysed by cross-correlating 50% overlapping windows of 32x32pixels, yielding fields of 77x61 vectors with a spatial resolution of 3.13 mm ($0.00224D$). For the 3C stereoscopic measurements, the Scheimpflug angular configuration, with the cameras placed on each side of the light sheet, was employed. Details of the procedure employed for the reconstruction of the three components can be found in Perrin & al (2006) and Cid & al (2002).

Time Resolved PIV measurements were carried out using a camera CMOS APX (PHOTRON) with a resolution of 1024x1024 pixels, and a laser Pegasus (New Wave) which delivers an energy of 2x10mJ. The system allows the acquisition of images pairs at a sampling rate of 1kHz. The camera was equipped with an 80mm objective lens at a diaphragm aperture of 1.8. As the laser is of lower energy than that used for the low data rate measurements, the size of the measuring domain was reduced to 67 x 92mm, located at ($0.76<x/D<1.24$, $-0.03<y/D<1.24$) as shown in Figure 6. The particle images were analysed using the above algorithm by cross correlating 50% overlapping windows of 64x64 pixels, giving a similar resolution to the low data rate PIV measurements.

2.3. Post-Processing

The time-independent mean motion issued from global averaging of the velocity fields are documented in the previous studies mentioned, and are not presented here with the exception of the time-independent stress tensor. These statistics were performed using about 3000 velocity fields.
In accordance with Reynolds & Hussain (1972), in the case of a periodic flow, phase averaging consists of a decomposition of the velocity which can be written as:

$$U_i = \overline{U_i} + \tilde{u}_i + u_i' = \langle U_i \rangle + u_i'$$

where $\overline{U_i}$ is the time-independent mean flow, $\tilde{u}_i$ is the quasi periodic fluctuating component, u_i' is the random fluctuating component, and $\langle U_i \rangle = \overline{U_i} + \tilde{u}_i$ is the phase averaged velocity.
As quasi periodic and random fluctuations are uncorrelated, the time-independent Reynolds stress tensor can then be written as the sum of a coherent contribution and a random one:

$$\overline{u_i u_j} = \overline{\tilde{u}_i \tilde{u}_j} + \overline{u_i' u_j'}$$

In the previous studies, phase averaging was performed using the pressure signal at an angular position of 70° to the forward stagnation point. This signal was chosen near the separation and upstream of the transition point, therefore containing a strong component at the Strouhal frequency (which is 22.5Hz, corresponding to a Strouhal number of 0.21) and is not too affected by turbulent fluctuations. From this signal, the phase angle of the vortex shedding was determined using the Hilbert transform. The velocity fields were then classified according to phase intervals of width 2p/128, and statistics were performed in these intervals. About 170 velocity fields were used at each phase angle to generate statistics.

As this procedure requires large data storage volumes and a long time of acquisition to obtain sufficient velocity fields at each phase angle, the phase averaged quantities were also obtained using the Linear Stochastic Estimation (Adrian (1975)), which allows the estimation of a conditional average from a non conditionally acquired data set. Generally, given one or several reference variables f_i, the conditional mean $\langle g \mid f \rangle$ of a variable g can be estimated as a linear function of f_i, using the correlation tensor. It is found by searching for the best estimation of g given f_i in the form:

$$g = A_j f_j$$

where A_j is given by $\overline{g f_k} = A_j \overline{f_j f_k}$. Here, the reference variables vector is constructed from the trigger signal as the trigonometric functions of the phase angle:

$$f = (e^{-jHj}, \ldots, e^{-jj}, 1, e^{jj}, \ldots, e^{jHj})$$

In Perrin & al (2006), this method was successfully applied to the non conditional data set of 2C PIV measurements, providing good agreement with the conditional sampling results, and then was applied to the 3-component data set to estimate the three-dimensional quantities in a phase averaged sense.

The POD analysis consists in searching for the function that is most similar to the members of a data set (Berkooz & al, (1991)). This is done by solving an eigenvalue problem where the kernel is the two point correlation tensor. The eigenvectors of this problem are the modes and the corresponding eigenvalues represents the energy contained by each modes. Given this basis of modes, the velocity fields can be reconstructed by projecting the instantaneous fields on a restricted number of modes. The reconstructed field can then be written as:

$$u_i = \sum_n a_n \Phi_i^{(n)} \quad \text{where} \quad a_n = \int_D u_i f_i^{(n)} dV$$

This decomposition is optimal in the sense that any reconstruction using another basis with the same number of modes contains less energy. Furthermore the diagonal decomposition of the two

point correlation tensor allow the Reynolds stresses to be written as

$$\overline{u_i u_j}(\vec{x}) = \sum_n l_n \Phi_i^{(n)}(\vec{x}) \Phi_j^{(n)*}(\vec{x})$$

Here, the POD was applied to the velocity fluctuations away from the mean fields. The snapshot method (Sirovich (1987)) was used with the 3000 instantaneous velocity fields of the low data rate PIV.

As a classical result for bluff body flows and as it will be seen in the next section, the first two modes of this decomposition present similar levels of energy, and are associated with the convection of the von Kármán vortices. Therefore, as carried out by Ben Chiekh & al (2004) and van Oudheusden & al (2005), the coefficients associated with these first two modes can be used to determine the phase angle of the vortex shedding. In the current paper, this definition of the phase angle has been used instead of that obtained from the pressure signal, and the phase averaged quantities have then been re-evaluated using LSE with the low sampling rate data set. The results of this processing are presented in Section 4.

3. Phase averaging and POD

The main results obtained from the phase averaging and POD are summarised. These decompositions are then analysed with the help of the TRPIV measurements.

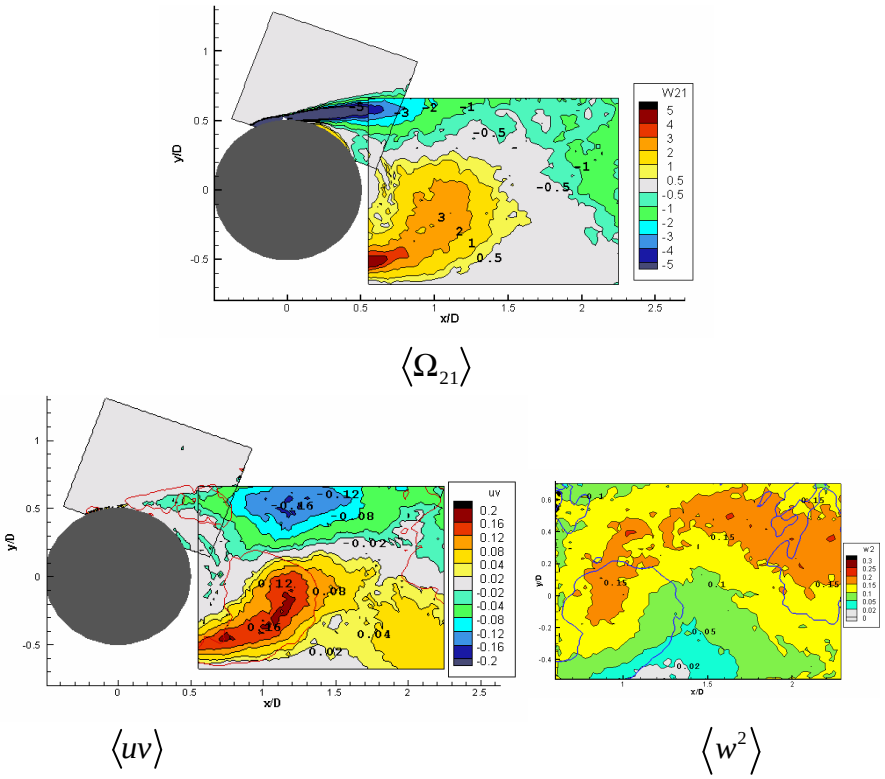

$\langle \Omega_{21} \rangle$ $\langle uv \rangle$ $\langle w^2 \rangle$

Figure 2. Phase averaged quantities at phase f =p/4 (with the pressure signal as reference signal)

Figure 2 shows the component $\langle \Omega_{21} \rangle$ of the rotation rate tensor, $\langle uv \rangle$ and $\langle w^2 \rangle$ at the phase angle $f = \pi/4$. The topology of the stresses in respect to the phase averaged motion is found to agree well with many other studies. In the region where the vortices begin to be convected, the highest values of the normal stresses $\langle u^2 \rangle$, $\langle v^2 \rangle$ and $\langle w^2 \rangle$ are located near the centre of the vortices, while the highest values of the shear stress $\langle uv \rangle$ are located between the vortices in the saddle

regions. In the very near region characterised by the formation of the vortices, high values of $\langle u^2 \rangle$ and $\langle uv \rangle$ are located in the separated shear layer, as expected. These high values then follow the motion of the vortices and are transported towards the centre of the wake. It is also noticeable that significant values of $\langle v^2 \rangle$ and $\langle w^2 \rangle$ are found in the regions connecting the vortices. This is presumably due to the presence of longitudinal vortices, connecting the primary ones. The general topology of these stresses is found in good agreement with the result of Cantwell & Coles (1983) and Hussain (1987), in the convection region of the von Kármán vortices, and those of Leder (1991), in the very near region, in the case of a vertical flat plate. The contributions of the quasi-periodic and random fluctuations to the time-independent shear stress $\overline{uv}$ are shown in Figure 3. In agreement with Cantwell & Coles, although the maxima of the random contribution are located slightly nearer the cylinder than the organised ones, these contributions are found to have similar topology and levels, despite the very different nature of the motions.

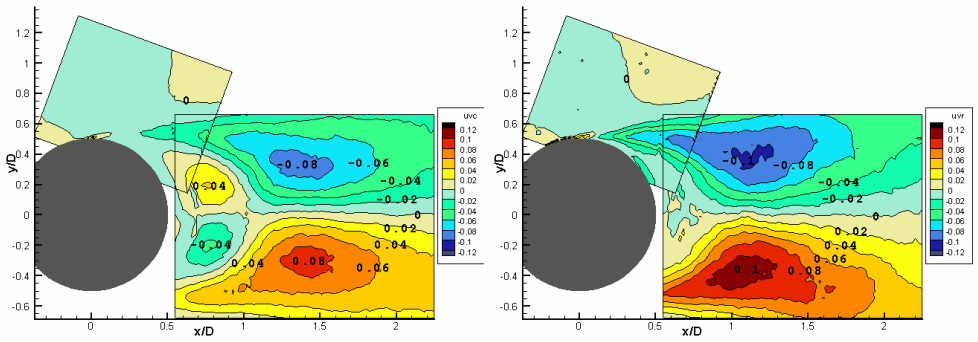

Figure 3. Organised *(left)* and random *(right)* contribution to the mean shear stress

POD was then performed to compare the coherent motion returned by both techniques. Figure 4a represents the percentage of the total energy of the fluctuating motion contained by each mode. It is seen that the two first modes have similar levels of energy, in accordance with other studies in the wake of a cylinder at lower Reynolds number (Deane & al (1991),...). The topology of these two modes is similar, with a shift in the x direction. Figure 4b shows the reconstruction of an instantaneous velocity field with different numbers of modes, *N*. As expected, the pattern of the von Kármán vortices is well reproduced. If we consider the task of extracting the coherent motion, the main difficulty lies in the choice of *N* to reconstruct it. Looking at the distribution of the energy, where a strong decrease is observed after *N*=10, and looking at the reconstruction of the instantaneous field, it seems that taking into account the 10 first modes would represent a good picture of the coherent motion. However, the choice of the modes should be determined in a more rigorous way than simple observation of the reconstructed fields.

To analyse these decompositions, TRPIV measurements were carried out in the very near wake, in a smaller domain, as shown in Figure 6. Validation was first carried out by comparing velocity spectra with those obtained by LDV in a companion study for the same flow conditions (Djeridi & al (2003)). An example spectrum is shown in Figure 5a, and it is seen that a very good agreement is achieved. In line with expectation, these spectra present a strong peak at the Strouhal frequency, corresponding to the von Kármán vortices, and a continuous part corresponding to the turbulent motion. From these measurements, streak-lines have also been calculated, by shedding particles on the upstream and lower sides of the measurement domain. Although, the calculation of these streak-lines is strongly biased because of the three-dimensionality of the flow, and are furthermore somewhat smoothed due to the resolution, it allows visualisation of the vortex shedding and the regions of high turbulence intensity with respect to the vortices.

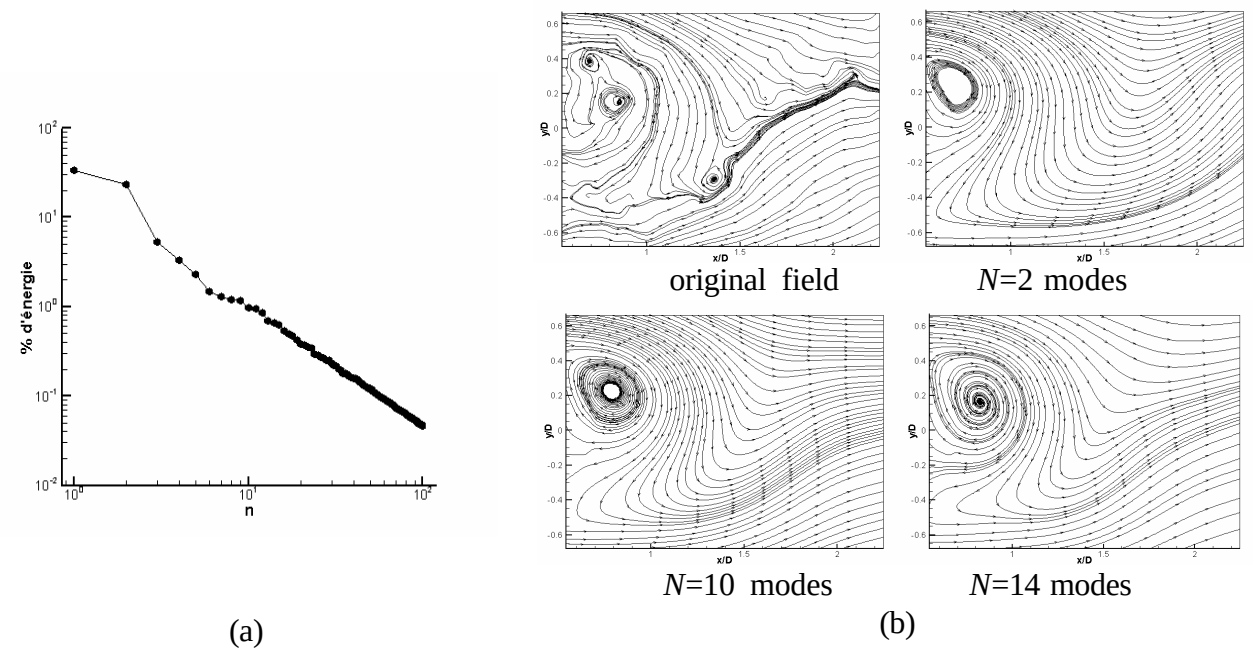

Figure 4. POD (a) energy of the modes (in % of the total energy of the fluctuating motion on the domain) ; (b) Example of reconstruction of an instantaneous field with *N* modes.

From these measurements, phase averaged quantities have been evaluated with the same procedure described above, using the pressure signal for determining the phase angle. Figure 6a shows the $<V>$ component of the phase averaged velocity obtained from low data rate PIV and Time Resolved PIV, demonstrating the good agreement achieved between these. Spectra of the fluctuating phase averaged component and the fluctuation away from the phase average are then evaluated. It is shown on Figure 6b that a residual peak remains in the spectrum of the so-called turbulent fluctuation, and the level of this peak is about 10% of the level of the Strouhal peak. In fact, this residual peak originates from phase lag occurring at certain instants between the pressure and velocity signals, which in turn gives rise to a small periodic component subsisting at some instants in the fluctuation away from the phase average. As a consequence, considering the contributions of the organised and random fluctuations to the time-independent Reynolds stress tensor, the contribution of the random fluctuation ought to be overestimated by the above phase averaged decomposition. To determine the extent of this overestimation, this contribution has been estimated by interpolating and integrating the continuous part of the velocity spectra. Figure 6c shows the contributions of organised and random motion evaluated from the spectra, and those evaluated from the phase average decomposition. As expected, the contribution of the random motion is overestimated, and the contribution of the organised fluctuation is underestimated.

Concerning the POD, it would have been interesting to plot spectra of the reconstructed velocity with the first *N* modes, and of the part corresponding to the rest of the modes. Unfortunately, the size of the TRPIV measurement domain is too small to perform a comparable POD to that of the low data rate acquisitions. Therefore, to analyse this decomposition, the contributions of the first *N* modes and the rest of the modes to the Reynolds stress tensor have been evaluated. Figure 7a and b show the contributions to $\overline{uv}$. In contrast to those obtained by phase averaging (Figure 3), the contributions have a different topology and magnitude, the contribution of the rest of the modes being mainly located, as expected, in the shear region. Figure 7c shows the contributions to $\overline{v^2}$ for different *N* and compared with those evaluated from the spectra. These contributions appear to be strongly dependent on the choice of *N*. Furthermore, it is found than, taking $N>2$ leads to an overestimation of the contribution of the coherent fluctuation.

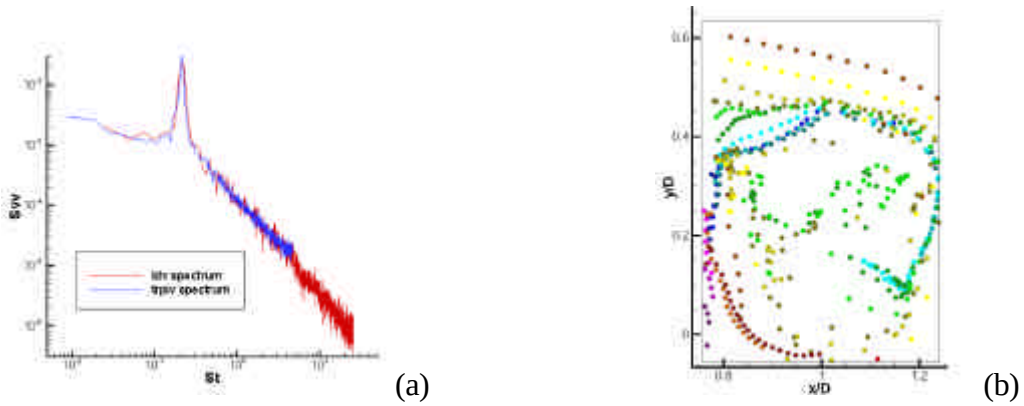

(a) (b)

Figure 5. TRPIV measurements. (a) spectrum of v fluctuation and comparison with LDV measurements); (b) Streak-lines

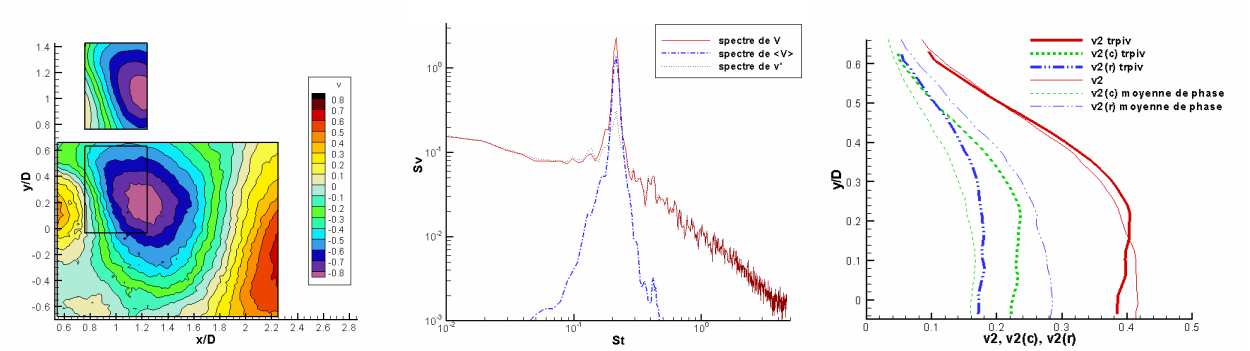

Figure 6. (a) Phase averaged velocity $<V>$ at f =p (the larger and smaller domains correspond to the low frequency and TRPIV measurements, respectively); (b) spectra of the quasi periodic and random fluctuations of v issued from the phase averaging with pressure signal at x/D=1, y/D=0.5; (c) contributions of these fluctuations to $\overline{v^2}$ at x/D=1(thick lines are the contributions evaluated from the spectra; solid lines (red) denote $\overline{v^2}$, dashed lines (green) denote the contributions of quasi-periodic fluctuations, solid dotted lines (blue) denote the random contributions).

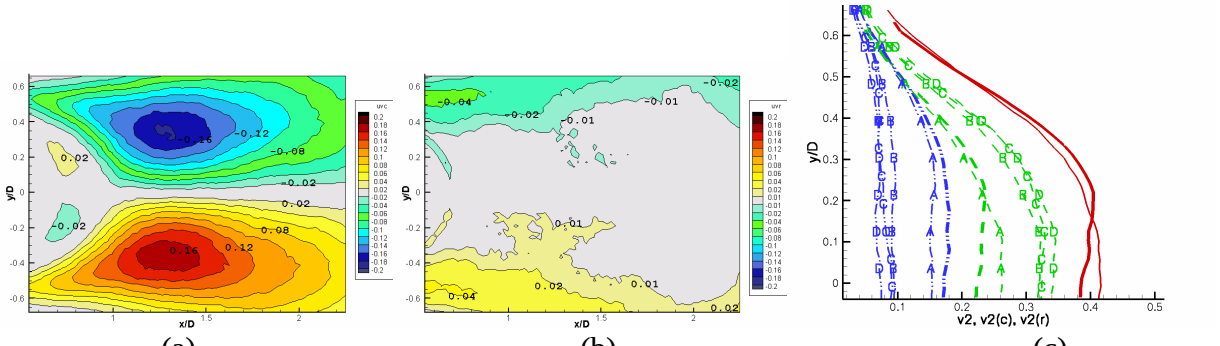

(a) (b) (c)

Figure 7. Decomposition of the Reynolds stresses by POD. (a) contribution of the 10th first mode to $\overline{uv}$ (b) contribution of the rest of the modes;
(c) decomposition of $\overline{v^2}$ at x/D=1 for different N compared with the organised and random contributions estimated from the spectra.
(thick lines are the contribution evaluated from the spectra; solid lines (red) denote $\overline{v^2}$, dashed lines (green) denote the contributions of the N first modes, solid dotted lines (blue) denote the contributions of the rest of the modes; A,B,C,D correspond to N=2, 6, 10 and 14 respectively)

4. Phase averaging using POD coefficients

It has been shown that the two first modes are linked to the convection of the vortices. Therefore, the coefficients obtained by projection of the instantaneous fields on the modes can be used to determine the phase of the vortex shedding, as demonstrated by Ben Chiekh & al (2004) and van Oudheusden & al (2005). The phase angle can then be given by:

$$j = \arctan\left(\frac{a_1/\sqrt{2l_1}}{a_2/\sqrt{2l_2}}\right)$$

In the current work, LSE has been used to re-evaluate the phase averaged quantities, using this definition of the phase angle instead of that of the pressure signal. As this phase angle is determined directly from the velocity fields to be averaged, it is expected that the effects of phase lag between the reference and velocity signals will be reduced. Figure 8 shows the $\langle\Omega_{21}\rangle$ component of the rotation rate tensor at phase angle $f = \pi/4$. By comparing Figures 8 and 2, it can be seen that the vortices are less smeared by the averaging process, indicating a reduction of the dispersion of the position of the vortices at a given phase angle. Furthermore, the topology of the coherent stresses seems to better follow the evolution of the vortices, as shown in Figure 10, especially in the regions of low turbulence intensity, at the border of the wake where external low-turbulence fluid is entrained towards the centre of the wake by the vortices. Finally, the contributions of the coherent and random fluctuations to the mean Reynolds stresses have also been re-evaluated. Figure 10a and b shows these contributions for the shear stress, which are more distinct than those evaluated from the previous phase averaging. Furthermore, the profiles of the contributions to $\overline{v^2}$, shown on Figure 10c, are in better agreement with those evaluated from the velocity spectra. These enhancements are a consequence of the determination of the phase angle directly from the velocity fields, thereby reducing the phase lag effects. Even if the general topology of the phase averaged quantities is the same as that of the phase averaged fields using the pressure signal, it is believed that a better decomposition of the flow into coherent and random parts is achieved.

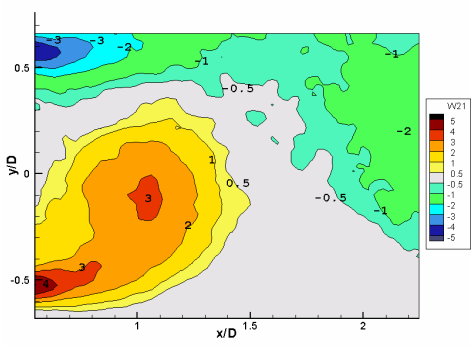

Figure 8. $\langle\Omega_{21}\rangle$ component of the rotation rate tensor at $f = p/4$ obtained by phase averaging using the POD coefficients

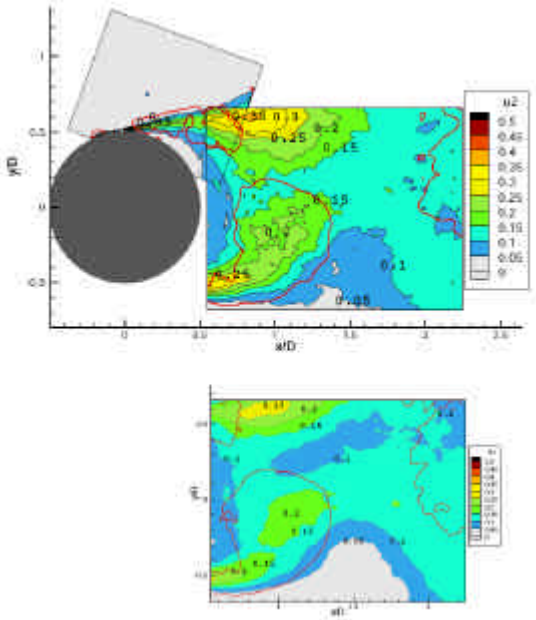

Figure 9. normal stress $\langle u^2\rangle$ at $f = p/4$, comparison between the phase averaging with pressure signal (above) and phase averaging with POD coefficient (below)

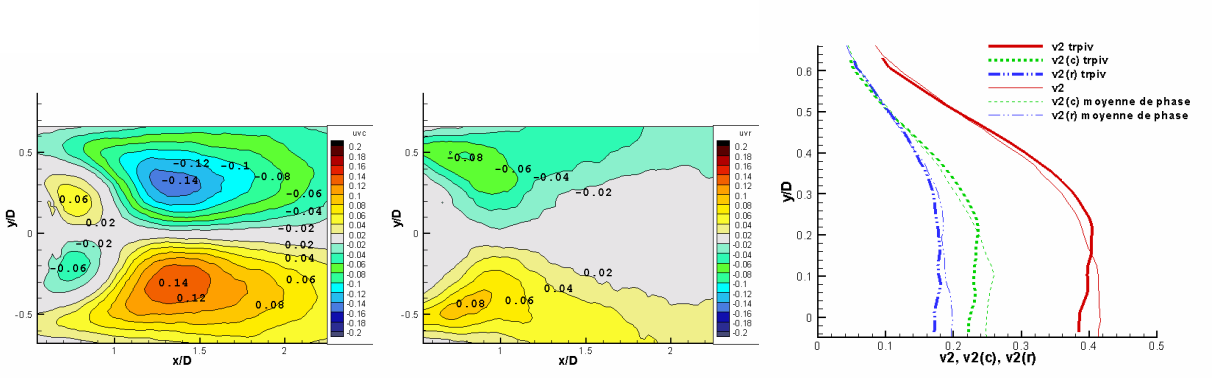

(a) (b) (c)

Figure 10. (a) and (b) Decomposition of the shear stress from phase averaging using POD coefficients. (c) Contributions of the organised and random fluctuations from phase averaging with POD coefficients compared with that evaluated from the spectra at *x/D*=1 (legend as in Figure 6c)

5. Comparison with a DES computation

As mentioned, this experimental study was conceived to provide a test case database for various computational methods under development, and is used as such in the EU FLOMANIA and DESider projects. A comparison with Detached Eddy Simulation (DES) results is briefly presented in this section, to illustrate the levels of comparability obtainable. The simulation has been conducted on a domain corresponding precisely to the experimental domain. The full grid used consists of some 5 million points. DES based on a compact explicit algebraic Reynolds stress (CEASM) RANS model has been used as implemented in the TU-Berlin in-house flow solver. The CEASM-DES formulation (Bunge & al (2005)) incorporates a mechanism to ensure that the entire turbulent boundary layer is handled by the RANS mode of the DES. The unsteady flow and turbulence field was saved every time step at the median plane corresponding to the experimental PIV measurements, and these snapshots are used to obtain global and phase-averaged fields using the same techniques described above. So far, an investigation of the time-step sensitivity of DES has been conducted, with two time-step sizes (0.03 & 0.05 *D/Uo*) computed. Figure 11a shows a typical instantaneous field (isosurfaces of l_2 coloured with the velocity *U*) obtained using the coarse time step, and allow visualisation of the longitudinal structures which the experimental topology of $\langle v^2 \rangle$ and $\langle w^2 \rangle$ suggests. Figure 11b shows a comparison of the phase-averaged $\langle \Omega_{21} \rangle$ at a phase angle of f =p/4, from which it can be seen that the position of the vortices agree well for the finer time-step, but are displaced further downstream with the coarse time step.

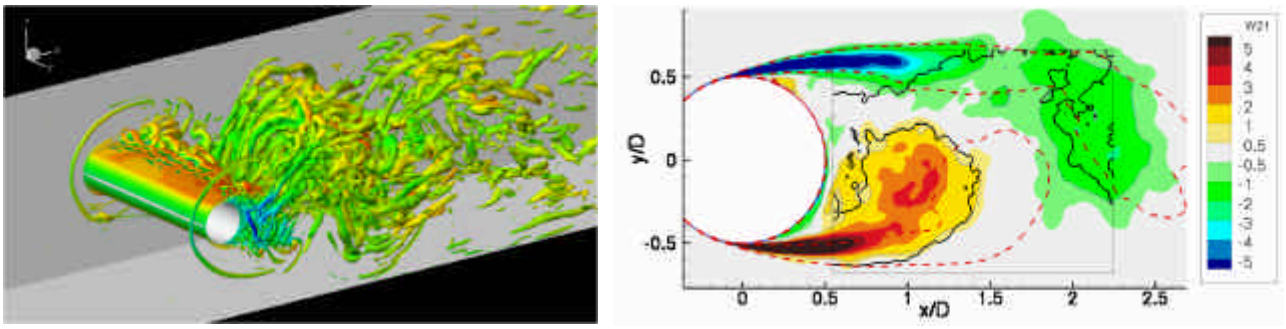

(a) (b)

Figure 11. (a) Instantaneous visualisation of flow-field from DES with coarse time-step, (b) Comparison of phase-averaged isolines of $\langle \Omega_{21} \rangle = \pm 1$ at f =p/4 between DES with fine time-step (colours and feint blue line), DES with coarse time-step (red dashed line) and PIV (solid black line).

6. Conclusion

In this study, the near wake of a circular cylinder at high Reynolds number and in a confined environment was investigated by means of PIV, stereoscopic PIV and Time Resolved PIV. Particular attention was paid to the decomposition of the flow in to organised and random motions. To this aim, phase averaging was used, allowing the evaluation of the mean fluctuating motion and the turbulent stresses. This was first achieved using the pressure signal on the cylinder to determine the phase of the vortex shedding. By analysing this decomposition with the help of TRPIV, it was found that phase lag occurring between the reference and velocity signals results in an overestimation of the random part of the motion. After comparing this decomposition of the flow with a POD analysis, the first POD coefficients were used to determine the phase of the vortex shedding, and the phase averaged quantities were re-evaluated. It was shown that the effect of the phase lag was alleviated because the phase angle is determined directly from the velocity fields to be averaged. A numerical simulation of the same flow has also been presented, for which an impressive level of agreement with the experiment has been demonstrated, which is attributed to the possibility of directly simulating the entire flow domain. An example of how the experimental data base can be used to quantify best practice guidelines for simulation has been presented.

Acknowledgement

The authors acknowledge the partial funding of the work presented here by the European Community during the DESider project, and by the German Research Foundation (DFG) within the scope of the Collaborative Research Center SFB 557.

The DESider project (Detached Eddy Simulation for Industrial Aerodynamics) is a collaboration between Alenia, ANSYS-CFX, Chalmers University, CNRS-Lille, Dassault, DLR, EADS-M, EUROCOPTER Germany, EDF, FOI-FFA, IMFT, Imperial College London, NLR, NTS, NUMECA, ONERA, TU Berlin, and UMIST. The project is funded by the European Community represented by the CEC, Research Directorate-General, in the 6th Framework Program, under Contract No. AST3-CT-2003-502842.

The DES computations were conducted on the IBM pSeries 690 at the Zuse-Institut Berlin (ZIB) and the Norddeutschen Verbund für Hoch- und Höchstleistungsrechnen (HLRN).

References

Adrian R. J. (1975) On the role of conditional averages in turbulence theory. In 4th biennal Symp. On Turbulence in Liquids.

Berkooz G., Holmes P. & Lumley J. L. (1993) The proper orthogonal decomposition in the analysis of turbulent flows. Ann. Rev. Fluid. Mech., 25: 539-575.

Ben Chiekh M., Michard M., Grosjean N., Bera J. C. (2004), Reconstruction temporelle d'un champ aérodynamique instationnaire à partir de mesures PIV non résolues dans le temps. In 9eme Congrès Fransophone de Vélocimétrie Laser.

Bloor M. (1964) Transition to turbulence in the wake of a circular cylinder. J Fluid Mech, 19: 290-304.

Braza M., Chassaing P. & Ha Minh H. (1990), Prediction of large-scale transition features in the wake of a circular cylinder, Phys. Fluids A, 2(8): 1461-1471.

Bunge, U. Mockett, C. & Thiele, F. (2005), Neue Hintergrundmodelle für die Detached-Eddy Simulation. Proceedings of the Deutscher Luft- und Raumfahrtkongress, DGLR-JT2005-212, p. 9.

Cantwell B. & Coles D. (1983) An experimental study of entrainment and transport in the turbulent wake of a circular cylinder. J Fluid Mech, 136: 321-374.

Cid E., Cazin S. & Drouin V. (2002) Validation de PIV stéréoscopique et application à un écoulement aérodynamique de sillage 3D, in 8eme Congres Francophone de Vélocimétrie Laser.

Deane A. E., Kevrekidis I. G., Karniadakis G. E. & Orzag S. A. (1991) Low-dimensional models for complex geometry flows: Application to grooved channels and circular cylinders. Phys. Fluids A 3, 2337-2354.

Djeridi H., Braza M., Perrin R., Harran G., Cid E. & Cazin S. (2003), Near wake turbulence properties around a circular cylinder at high Reynolds number. Flow, Turbulence and Combustion, 71: 19-34.

Kourta A. Boisson H. C. Chassaing P. & Ha Min H. (1987) Nonlinear interaction and the transition to turbulence in the wake of a circular cylinder. J Fluid Mech, 181: 141-161.

Leder A. (1991) Dynamics of fluid mixing in separated flows. Phys Fluis A, 3(7): 1741-1748

Lumley J. L. (1967) The structure of inhomogeneous turbulent flows. In Atmospheric Turbulence and Radio Wave Propagation, ed A. M. Yaglom, V. I. Tatarski, Nakua, Moscow, 166-178.

Perrin R., Braza M., Cid E., Cazin S., Moradei F., Barthet, Sevrain A. & Hoarau Y. (2005) Near-wake turbulence properties in the high Reynolds incompressible flow around a circular cylinder by 2C and 3C PIV, in proc. of 6th ERCOFTAC International Symposium on Engineering Turbulence Modelling and Measurements, ETMM6, May 23-25, Italy, Sardinia, selected for a special issue of Flow Turbulence & Combustion, in press.

Perrin R., Cid E., Cazin S., Sevrain A., Braza M., Moradei F., Barthet, & Harran G. (2006) Phase averaged measurements of the turbulence properties in the near wake of a circular cylinder at high Reynolds number by 2C-PIV and 3C PIV, accepted for publication, in revision for Experiments in Fluid.

Persillon H. & Braza M. (1998) Physical analysis of the transition to turbulence in the wake of a cylinder by three-dimensional Navier-Stokes simulation. J Fluid Mech, 365: 23-88.

Sirovich L. (1987) Turbulence and the dynamics of coherent structures. Part I, II & III. Quarterly of Applied Mathematics XLV(3):561-582.

Van Oudheusden, Scarano F., Van Hinsberg & Watt D. W. (2005) Phase resolved characterisation of vortex shedding in the near wake of a square-section cylinder at incidence. Experiment in Fluids.

Williamson C. H. K. (1992) The natural and forced formation of spot-like vortex dislocations in the transitio of a wake. J Fluid Mech, 243:393-441.